Dalton Transactions

ROYAL SOCIETY OF CHEMISTRY

PAPER

View Article Online
View Journal | View Issue

Cite this: *Dalton Trans.*, 2025, **54**, 11563

Synthesis, electronic properties, structural studies, and catalytic activity of peripherally metalated β-η^1-Pd(II)-thioalkyl porphyrazine†

Sandra Belviso, *[a] Giuseppe Larotonda, [a] Ernesto Santoro, [a] Alessandro Santarsiere [a] and Angela Tuzi [b]

The β-η^1-Pd(II)-thioethyl porphyrazine complex **1** was isolated as an intermediate in the Suzuki–Miyaura cross-coupling of β-bromo thioethyl porphyrazine with palladium complexes. The same complex was also synthesized *via* a direct reaction of the bromo porphyrazine with $Pd(PPh_3)_4$ and its structure was assessed by NMR and single-crystal X-ray diffraction analysis, representing one of the very few cases of crystallographic resolution of a thioalkyl porphyrazine obtained to date. This organometallic thioethyl porphyrazine derivative constitutes the first example of an η^1 organometallic complex of tetrapyrroles in which the metal is coordinated at the β position of the macrocycle rather than at the *meso* position, as observed in some porphyrin complexes. Spectroscopic and electrochemical studies, including UV-vis absorption and cyclic voltammetry, supported by time-dependent density functional theory calculations revealed that compared to symmetrically substituted thioalkyl porphyrazines, this complex exhibits a reduced HOMO–LUMO bandgap and a charge transfer transition involving the metal and the macrocycle at the typical tetrapyrrole Soret band. This behavior markedly contrasts with that observed in peripherally aryl-substituted thioalkyl porphyrazines, where a charge transfer HOMO–LUMO transition occurs between the aryl substituent and the macrocycle core in correspondence to the Q bands region. Furthermore, the complex demonstrated good catalytic activity in both Suzuki–Miyaura and Sonogashira Pd(II)-catalyzed coupling reactions of aryl halides with boronic acids or alkynes, respectively. In both reactions, the porphyrazine complex performed with comparable efficiency to the commonly used $Pd(PPh_3)_2Cl_2$ catalyst.

Received 13th June 2025,
Accepted 7th July 2025

DOI: 10.1039/d5dt01394a

rsc.li/dalton

Introduction

Tetrapyrroles asymmetrically substituted at the periphery of the macrocycle exhibit highly delocalized π-electron systems, making them ideal structural frameworks for the development of materials with non-linear optical (NLO) properties[1] or as dyes for organic photovoltaic (OPV) applications.[2,3] In particular, the selective incorporation of aromatic moieties with appropriate electronic properties can extend molecular conjugation thereby enabling "push–pull" systems suitable for NLO applications.[4] While peripheral structural modifications and their related optoelectronic applications have been extensively investigated for the most common tetrapyrroles such as porphyrins[2] and phthalocyanines,[3] the structurally analogous subgroup of porphyrazine macrocycles has been comparatively underexplored in the NLO[5] and OPV[6] fields. However, porphyrazines offer several advantages, including greater structural tunability and significant spectral absorbance aligned with the most intense regions of the solar emission spectrum. Consequently, in recent years, we have focused on developing aryl-substituted porphyrazines possessing tailored structural and electronic properties for application in both NLO and OPV fields. Initially, we synthesized various aryl- and arylethynyl-substituted thioalkyl porphyrazines, wherein both electron-donating and electron-withdrawing groups markedly influenced the molecular charge distribution.[7] In these compounds, the macrocycle can function either as an electron acceptor or a donor depending on the nature of the substituents, resulting in an unconventional "push–pull" system.[8] In such a system, the presence of charge transfer HOMO–LUMO transitions between spatially distant moieties of the molecule can prevent exciton recombination, thereby prolonging the exciton lifetime. We then described the first efficient photovoltaic device based on nanocomposites composed of a pyrene-

[a]*Dipartimento di Scienze di Base e Applicate, Università della Basilicata, Via dell'Ateneo Lucano 10, 85100 Potenza, Italy. E-mail: sandra.belviso@unibas.it*
[b]*Dipartimento di Scienze Chimiche, Università degli Studi di Napoli Federico II, Via Cintia 21, 80126 Napoli, Italy*

†Electronic supplementary information (ESI) available: SCXRD experimental data and figures, TDDFT computed molecular orbitals, dipolar and rotational strengths of electronic transitions, and synthetic details. CCDC 2455381. For ESI and crystallographic data in CIF or other electronic format see DOI: https://doi.org/10.1039/d5dt01394a

substituted thioalkyl porphyrazine combined with both carbon nanotubes and graphene.[9,10] Finally, we reported a new porphyrazine scaffold conjugated with an extended aromatic hexahelicene moiety endowed with inherent chirality.[11] In these studies, the aryl-substituted porphyrazines were synthesized *via* Pd(0)-catalyzed Suzuki–Miyaura[12] or Sonogashira[13] cross-coupling reactions starting from mono-brominated thioalkyl porphyrazines. In the Suzuki–Miyaura reaction between the β-bromo thioethyl porphyrazine **H_2SC_2Br** and a generic aryl boronic acid (Scheme 1), good yields of the aryl-substituted porphyrazine product were typically obtained. However, a minor secondary product frequently isolated from the crude mixture was identified, using ^{1}HNMR and ^{13}CNMR analyses, as the β-η^1-Pd(II)-thioethyl porphyrazine complex **1** (Scheme 2). This complex arises from the oxidative addition of the parent β-bromo porphyrazine to the $Pd(PPh_3)_4$ catalyst and can be considered the first intermediate in the catalytic cycle of the cross-coupling reaction. The amount of the recovered complex depended on the reaction time and solvent used: when employing a DMF/toluene mixture, yields were less than 1%, whereas reactions carried out in THF afforded up to 5% yield.

Some *meso* ring-metalated porphyrins have been reported previously as by-products of cross-coupling reactions,[14] while only a single example of a β cyclometalated porphyrin dimer has been described.[15] Therefore, complex **1** represents the first example of an isolable β-ring-metalated tetrapyrrole. We subsequently undertook a comprehensive structural and reactivity study of this compound to elucidate its role in the aforementioned cross-coupling reaction. Accordingly, the direct synthesis of complex **1**, its structural characterization, and a detailed investigation of its spectral and electrochemical properties by both experimental and computational methods, as well as its application as a catalyst in cross-coupling reactions are herein reported.

Results and discussion

Synthesis

In order to carry out detailed structural and reactivity studies on complex **1**, it was first necessary to establish a suitable synthetic strategy for its direct preparation. Accordingly, the mono-brominated thioethyl porphyrazine **H_2SC_2Br** was synthesized starting from the symmetrically substituted porphyrazine **H_2SC_2** [16] through a multi-step procedure involving the removal of one ethylsulfanyl chain yielding the nonsymmetrical β-H-substituted porphyrazine,[17] followed by a selective mono-bromination.[18] This unique *a posteriori* asymmetrization process of the symmetric parent macrocycle avoids the commonly low yielding statistical macrocyclization. Subsequently, complex **1** was smoothly obtained in 80% yield by reacting the brominated porphyrazine **H_2SC_2Br** with an equimolar amount of $Pd(PPh_3)_4$ in refluxing toluene (Scheme 2).

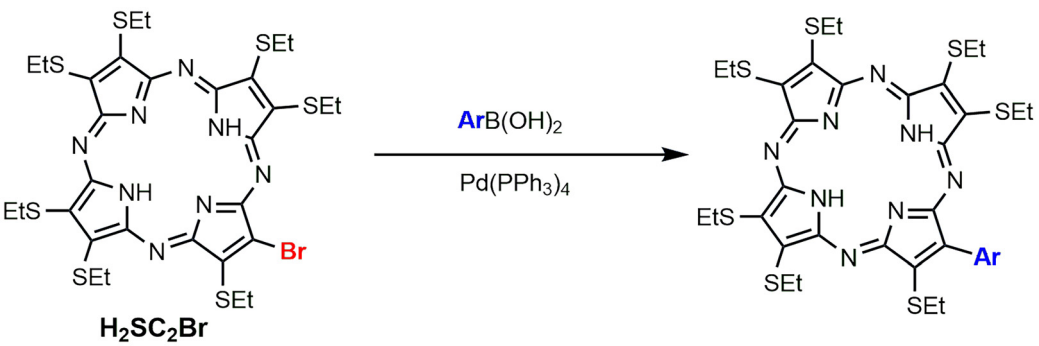

Scheme 1 General scheme for aryl-substituted thioethyl porphyrazine synthesis through Suzuki–Miyaura cross-coupling.

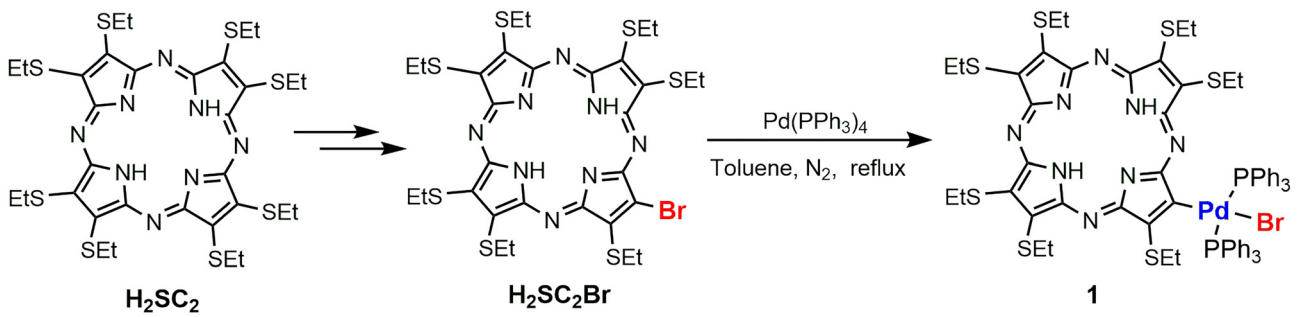

Scheme 2 Direct synthesis of β-η^1-Pd(II)-thioethyl porphyrazine complex **1**.

Structural characterization of the complex 1

The ^{1}HNMR spectrum of **1** (Fig. 1) shows the typical signals of a "free base" asymmetric thioethyl porphyrazine. In fact, at −1.85 ppm, a singlet (*a*) allied to the internal protons of the macrocycle; between 1.0 and 2.0 ppm, the signals (*b*) of 21 protons of the methyl groups of the thioethyl chains appearing either as triplets or multiplets; and between 3.5 and 4.5 ppm, three quartets and a multiplet (*c*) allied to the 14 protons of the –SCH_2 groups of the chains are observed. Finally, three intense signals (*d*) corresponding to 6, 12, and 12 protons are observed in the aromatic zone which could be attributed to the *para*, *meta*, and *ortho* protons of the six phenyl groups of the two triphenylphosphine moieties.

The ^{13}CNMR spectrum confirms the presence of the triphenylphosphine moieties together with the thioethyl substituted porphyrazine system (Fig. 2). In fact, in the spectrum there are two signals attributable to aliphatic carbons, respectively, around 15 and 30 ppm, while in the aromatic zone, four intense signals can be observed between 120 and 135 ppm, followed at the lower field by numerous signals of the quaternary carbons of the macrocycle. The detailed analysis of the signals between 120 and 135 ppm (Fig. 3) shows two flared singlets at 127.3 (*c*) and 129.6 ppm (*d*), followed by two triplets at 130.4 (*a*) and 134.5 ppm (*b*). These triplets can be attributed to the *ipso* and *ortho* carbons of the phenyls of triphenylphosphine. Their multiplicity indicates the presence of a coupling with two ^{31}P nuclei, the one adjacent to the phenyl and, through a "virtual coupling", the one belonging to another triphenylphosphine moiety, constituting an ABX spin system. On the basis of what is reported in the literature for the phosphine complexes of Pd and Pt,[19,20] this spectral pattern can be attributed to the presence of two PPh_3 groups coordinated in the *trans* position to a Pd atom in turn linked to the macrocycle.

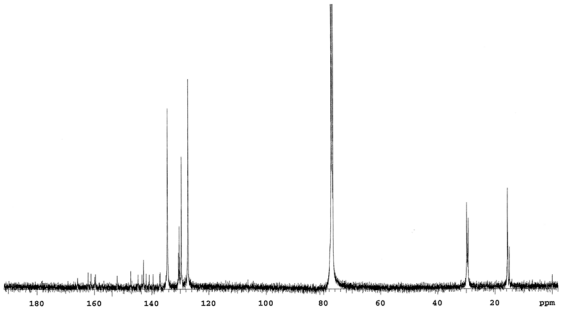

Fig. 2 ^{13}C NMR spectrum ($CDCl_3$) of complex **1**.

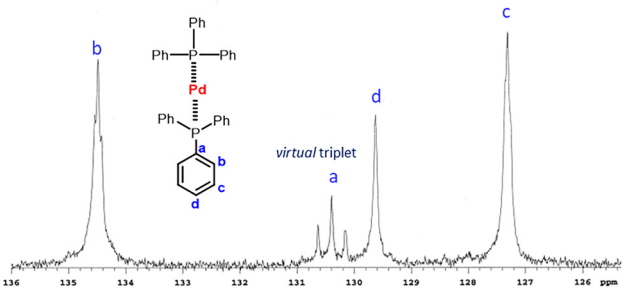

Fig. 3 ^{13}CNMR spectrum ($CDCl_3$) of complex **1**. Enlargement of the 126–136 ppm range.

Further confirmation of the presence of phosphorus atoms in complex **1** is obtained from the ^{31}PNMR spectrum (Fig. S1 in the ESI†), in which the presence of a singlet at 24 ppm is clearly evident. The above spectroscopic data confirm the formation of the organometallic β-η^1-Pd(II)-thioethyl porphyrazine *trans* complex **1** (Scheme 2), *i.e.* the intermediate of the catalytic cycle of the cross-coupling reaction coming from the oxidative addition

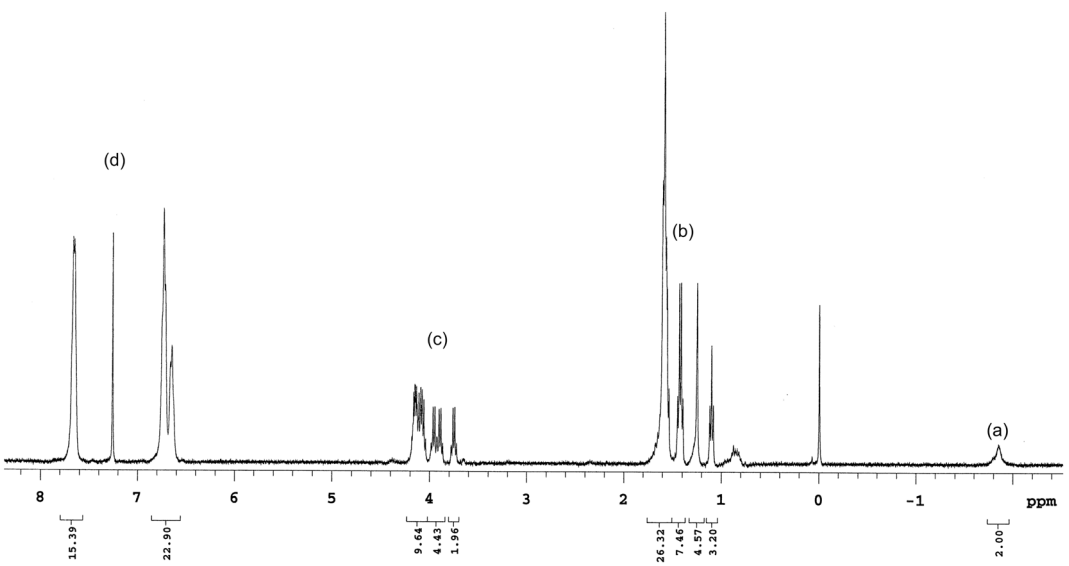

Fig. 1 ^{1}H NMR spectrum ($CDCl_3$) of complex **1**.

of bromo porphyrazine **H_2SC_2Br** to the Pd(0) catalyst $Pd(PPh_3)_4$. Notably, complex **1** was particularly stable in air and in solution, allowing its crystallization from a CH_2Cl_2/MeOH mixture.

Crystallographic analysis

Single crystals of complex **1** suitable for single-crystal X-ray diffraction (SCXRD) analysis were obtained by slow diffusion of methanol in a CH_2Cl_2 solution followed by a very slow evaporation of solvent at ambient temperature. Complex **1** (Fig. 4 and Fig. S3 in the ESI†) crystallizes in the triclinic $P\bar{1}$ space group with one molecule of the complex and one dichloromethane solvent molecule contained in the asymmetric unit. Bond lengths and bond angles are in the normal range and in agreement with similar compounds.[21]

The molecular structure of the compound confirms that the halogenated $-PdBr(PPh_3)_2$ group is in the β position of a pyrrole ring and that a partial exchange of the Br atom with the Cl atom took place during crystallization, with the two molecular structures being different only due to the nature of the halogen. In fact, as reported in the literature,[21c] during the slow crystallization process of brominated complexes, the presence of chlorinated solvents can induce a partial exchange of the halogen. The structural analysis showed that the halogen exchange was almost complete and that only a very small fraction of the brominated to the chlorinated compound was formed (the fraction of –Cl to –Br is 0.98 to 0.02).

The complex exhibits the usual square planar geometry around the Pd atom, with the square plane approximately perpendicular to the porphyrazine ring system. The C–Pd–halogen axis is in the plane of the pyrrole ring and the two $-PPh_3$ groups are arranged in approximately mirror symmetry with phenyl rings overlapping the pyrrole ring on both sides. The pyrrolic hydrogen atoms in the porphyrazine ring system, identified with certainty in the Fourier difference maps, show a *trans* disposition of the NH groups that are involved in the usual intramolecular N–H···N hydrogen bonding pattern observed in similar compounds. The porphyrazine ring system is essentially planar and assumes a slightly-bent flat shape with the peripheral thioethyl groups alternatively oriented up-plane and in-plane with it (Fig. S4 and S5 in the ESI†). Less encumbrance on one side of the macrocyclic porphyrazine ring is observed, due to the preferential disposition of the ethyl groups that protrude from the same side of the porphyrazine plane (Fig. S6 in the ESI†). The crystal packing is stabilized by normal van der Waals interactions and face-to-edge interactions of phenyl rings. The crystallographic structure confirms the spectroscopic data obtained: the intermediate formed is an organometallic complex, the metal atom is linked to the β position of the macrocycle and the two $-PPh_3$ groups linked to the metal atom are positioned in *trans*; also the presence of bromine was confirmed. Furthermore, it is visible that the geometry of the complex formed by Pd(II) is, as expected, of the square planar type. This structure represents one of the very few cases of crystallographic resolution obtained so far for a thioalkyl porphyrazine. Above all, it is important to note that complex **1** represents the first example of a tetrapyrrole η^1 organometallic complex having a Cβ–M bond.

Spectroscopic analysis

Detailed studies of the spectral and electrochemical properties of complex **1** have also been carried out. Its UV-vis absorption spectrum in CH_2Cl_2 is shown in Fig. 5, together with that of the symmetrically substituted thioethyl porphyrazine **H_2SC_2**. The spectrum of **1** shows several intense absorption bands in the 250–800 nm range featuring the typical characteristics of non-aggregated "free base" thioalkyl porphyrazines[22] and closely resembling that of **H_2SC_2**, but with distinctive differences in the wavelengths of the two Q bands.[23] Specifically, the main spectral features of **1** are the two Q bands at 693 nm and 650 nm, the "extra" band at 515 nm (due to the $n_{sulfur} \rightarrow \pi^*$ transitions),[24] and the Soret band at 363 nm. Moreover, a new band at 307 nm, attributable to the triphenylphosphine

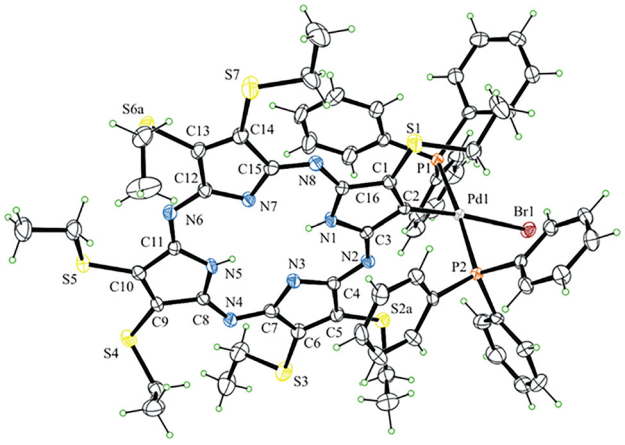

Fig. 4 ORTEP view of complex **1** with ellipsoids drawn at 50% probability level. The dichloromethane solvent molecule and the minor parts of the disordered thioethyl groups have been omitted for clarity.

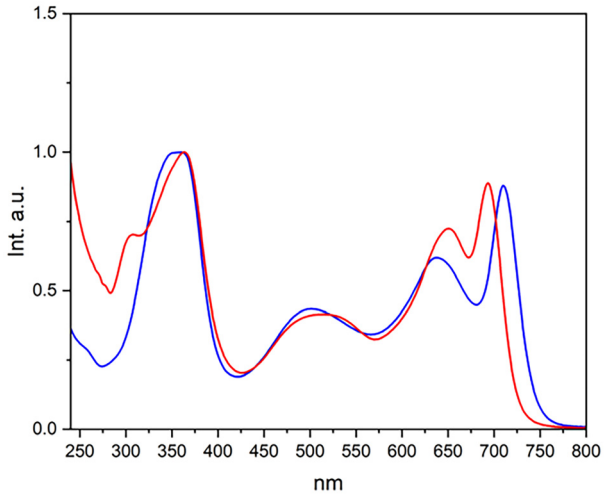

Fig. 5 UV-vis absorption spectra (CH_2Cl_2) of compound **H_2SC_2** (blue line) and complex **1** (red line).

chromophore, is present. A comparison of the experimental spectra of both species (Fig. 5) highlights differences arising from the modification of the macrocycle periphery. The most notable differences include a blue-shift (~17 nm) of the lower energy Q_x band of **1** and a red-shift (~13 nm) of the higher energy Q_y band. Additionally, red-shifts of both the "extra" band (~15 nm) and Soret band (~4 nm) are observed.

To gain further insight into the electronic structure of complex **1**, a time-dependent density functional theory (TDDFT) computational investigation was performed to interpret the UV–vis spectral features by comparing the main transitions with those of the parent unsubstituted porphyrazine $\mathbf{H_2SC_2}$. Accordingly, quantomechanical calculations at the TDDFT/ωB97X-D3/def2-TZVP/CPCM(CH_2Cl_2) level of theory were carried out on both $\mathbf{H_2SC_2}$ and **1**. The UV-vis transitions of $\mathbf{H_2SC_2}$ have been previously described and assigned with computational support,[24] but for consistency in spectral comparison, these calculations were repeated at the same level of theory used for complex **1**. Overall, the interpretation of the main electron transitions in $\mathbf{H_2SC_2}$ confirmed earlier reports, with an improved match to the experimental data (Fig. 6). The two Q_x and Q_y bands at 673 and 648 nm correspond to the HOMO → LUMO and HOMO → LUMO+1 MO transitions, respectively (see Fig. 7 right side and Table S3 in the ESI†). The "extra" band can be ascribed to two main transitions (#6 and #9 in Table S3 in the ESI†): the first involves the HOMO−1 → LUMO transition, with the charge transfer (CT) character localized on sulfur electrons, while the second results from combined HOMO−3 → LUMO+1 and HOMO−2 → LUMO+1 CT transitions covering different sulfur localized orbitals. The Soret band is described by π–π* transitions, #17–19, originating from the combination of HOMO−6/−7/−8 → LUMO/LUMO+1 and #27 by HOMO−13/HOMO−12 → LUMO+1. This new set of calculations aligns well with experimental data, closely matching relative intensities and positions of the Q_x and Q_y bands, the origin of the characteristic "extra" band of the thioalkyl porphyrazines, and the relative intensity of the Soret band.

For complex **1**, the computed dipolar strengths superposed on the experimental UV-vis spectrum (Fig. 8) well reproduce

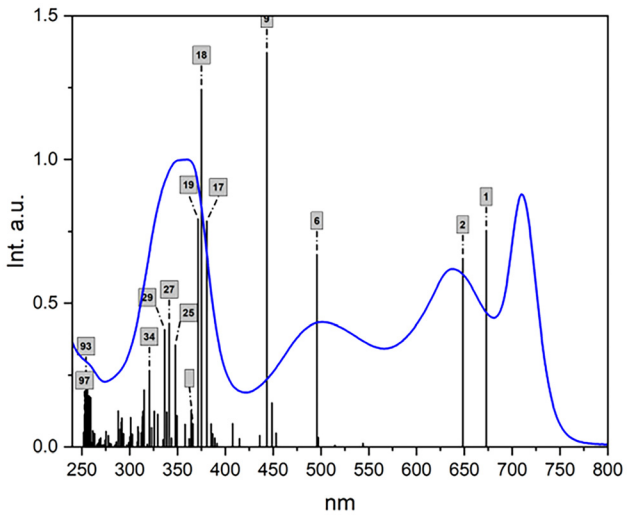

Fig. 6 Experimental UV-vis spectrum (blue line) and computed dipolar strengths (black bars) at the TDDFT/ωB97X-D3/def2-TZVP/CPCM (CH_2Cl_2) level of theory for $\mathbf{H_2SC_2}$.

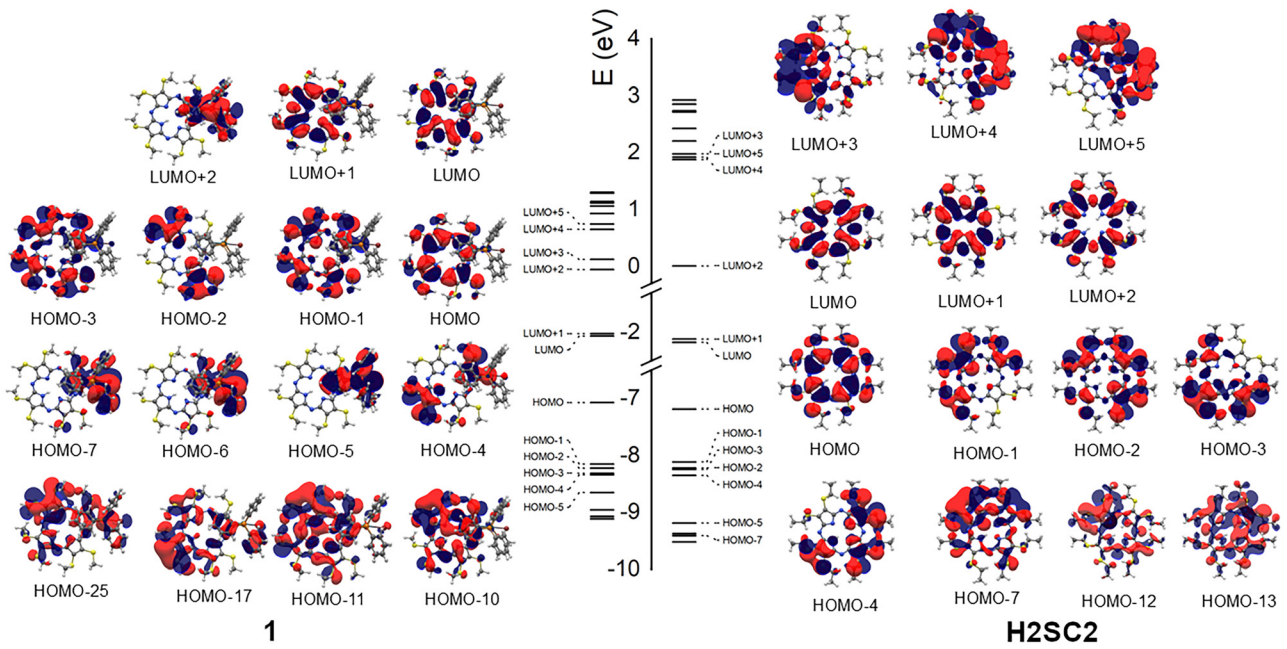

Fig. 7 Kohn–Sham orbital energy levels and graphical representations of some more relevant orbitals computed at TDDFT/ωB97X-D3/def2-TZVP/CPCM (CH_2Cl_2) for $\mathbf{H_2SC_2}$ (right side) and complex **1** (left side).

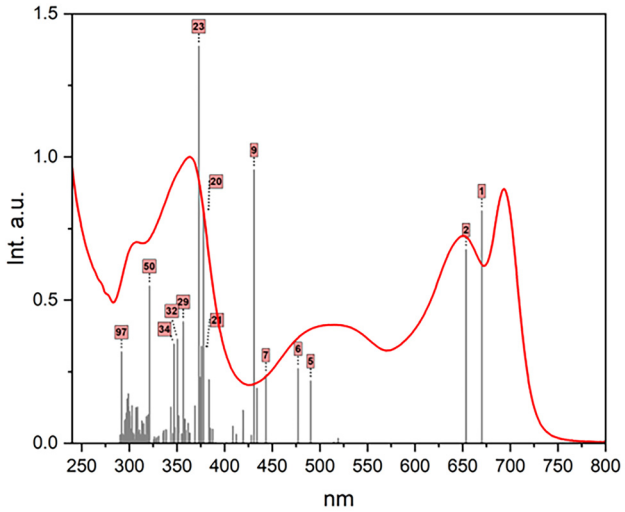

Fig. 8 Experimental UV-vis spectrum (red line) and computed dipolar strengths (grey bars) at the TDDFT/ωB97X-D3/def2-TZVP/CPCM (CH_2Cl_2) level of theory for **1**.

the observed main spectral features in terms of position and relative intensity. Both Q_x and Q_y bands derive from a combination of the HOMO → LUMO and HOMO → LUMO+1 transitions (transitions #1 and #2 in Table S4 in the ESI†) localized on the macrocycle core (Fig. 7 left side). With respect to $\mathbf{H_2SC_2}$, a different mixing probability of the MO character, due to a smaller energy gap between nearly degenerate LUMO and LUMO+1, and a smaller $\Delta E_{HOMO-LUMO}$ bandgap (5.0078 eV (**1**) *vs.* 5.0127 eV ($\mathbf{H_2SC_2}$)), are observed. The calculations reproduce the convergence of the two Q bands, resulting from a blue-shift of the Q_x band and a red-shift of the Q_y band. In the 420–550 nm range, a higher number of transitions (#5–9, Fig. 7 left side, Table S4 and Fig. S7 in the ESI†) occur from HOMO−1 to HOMO−4 MOs localized on peripheral sulfur atoms to the macrocycle core LUMO+1, reflecting the reduced molecular symmetry. Notably, the transitions contributing to the Soret band (transitions #20, 21, and 23 in Table S4 in the ESI†) have different origins and characteristics: transition #23 (HOMO−10 → LUMO+1) is fully localized on the macrocycle, whereas both transitions #20 (HOMO−5 → LUMO) and #21 (HOMO−5 → LUMO/LUMO+1) involve CT from the HOMO−5 MO localized on the $Pd(PPh_3)_2$ substituent (Fig. S8 in the ESI†) to the LUMO/LUMO+1 MOs localized on the macrocycle core (Fig. 7 left side). It is worth noting that in peripherally aryl-substituted thioalkyl porphyrazines[7–9,11] HOMO–LUMO CT transitions occur between the aryl substituent and the macrocycle core, whereas in complex **1** the CT transition occurs at higher energy, in correspondence to the Soret band. Finally, the additional feature at 307 nm corresponds to transition #50 (HOMO−7 → LUMO+2) attributable to a π–π* transition localized on the triphenylphosphine groups.

Electrochemical properties

The electrochemical behavior of the novel Pd(II) porphyrazine complex **1** was investigated. The analysis was carried out using cyclic voltammetry (CV) and differential pulse voltammetry (DPV) with all potentials (Table 1) reported *versus* the ferro-

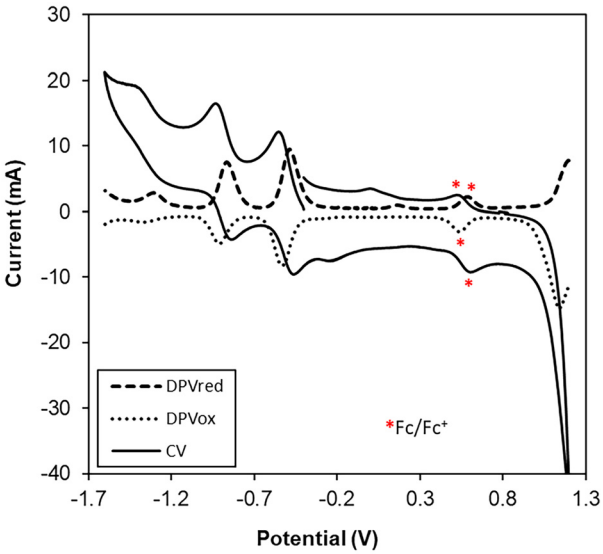

Fig. 9 Cyclic voltammogram and differential pulse voltammograms of complex **1** in CH_2Cl_2. Ferrocene/ferrocenium redox signals are labeled with a red asterisk.

Table 1 Summary of the peak potentials $E_{1/2}$ (volts *vs.* Fc/Fc^+) for complex **1** and compound $\mathbf{H_2SC_2}$

				Reduction		E_{HOMO} [b]		E_{LUMO} [b]		
Compd	Tech[a]	Solvent	Oxidation	I	II	Expt.	Compt[c]	Expt.	Compt[c]	HOMO–LUMO bandgap
1	(CV)	CH_2Cl_2	—	−1.077	−1.454		−5.792[d]	−3.723	−3.337[d]	—
	$(DPV)_{red}$	CH_2Cl_2	—	−1.076	−1.458			−3.724		—
	$(DPV)_{ox}$	CH_2Cl_2	—	−1.068	−1.446			−3.732		—
	(CV)	DMF	—	−0.929	−1.381			−3.871		—
	$(DPV)_{red}$	DMF	0.713	−0.934	−1.409	−5.513	−5.729[e]	−3.866	−3.273[e]	1.647
	$(DPV)_{ox}$	DMF	0.714	−0.911	−1.389	−5.514		−3.889		1.625
$\mathbf{H_2SC_2}$	(CV)	CH_2Cl_2	—	−0.907	−1.230			−3.893		—

[a] Measured in 10^{-3} M solution with a glassy carbon working electrode. [b] Values (eV) refer to first oxidation and first reduction, and are calculated assuming the energy level for the ferrocene at −4.8 eV.[28,29] [c] HOMO and LUMO orbital energy calculated by DFT on the optimized neutral molecule. [d] TDDFT/M06/def2-TZVP/CPCM(CH_2Cl_2). [e] TDDFT/M06/def2-TZVP/CPCM(DMF).

cene/ferrocenium redox couple used as the internal standard. The redox profile of complex **1** is typical of thioalkyl porphyrazines. As can be seen from the cyclic voltammogram shown in Fig. 9, the cathodic curve is characterized by two reversible monoelectronic processes[25] of reduction of the porphyrazine ring attributed to the formation of the porphyrazine π-anion radical and dianion, respectively.[26,27] The half-wave potentials in CH_2Cl_2 for these two processes are, respectively, $E_{1/2}(\Delta E_p)$ = −1.077 V (0.072) and $E_{1/2}(\Delta E_p)$ = −1.454 V (0.073). The ΔE_p values, slightly higher than the theoretical 0.057 V, indicate quasi-reversible processes.

The DPV data are consistent with the CV results. The electrochemical analysis in DMF provided reduction potential values very similar to those in CH_2Cl_2, and allowed detection of the oxidation potential not clearly visible in the latter solvent (Table 1). HOMO and LUMO energies calculated from the electrochemical data are reported in Table 1, by assuming the energy level of ferrocene/ferrocenium to be −4.8 eV.[28–30] The HOMO and LUMO energies calculated from the experimental electrochemical data are −5.5 eV for the HOMO and −3.9 eV for the LUMO, respectively, yielding a bandgap of approximately 1.6 eV. As observed for other asymmetrically substituted thioalkyl porphyrazines, these HOMO and LUMO energy values make **1** potentially suitable for fabrication of BHJ cells with nanocarbon acceptors.[9,11] A significant shift to more cathodic values is observed in the case of complex **1** compared to the potential values of the "free base" porphyrazine $\mathbf{H_2SC_2}$. Computed values for the HOMO and LUMO energies at the TDDFT/M06/def2-TZVP/CPCM level of theory in both CH_2Cl_2 and DMF are also reported in Table 1. They are in good

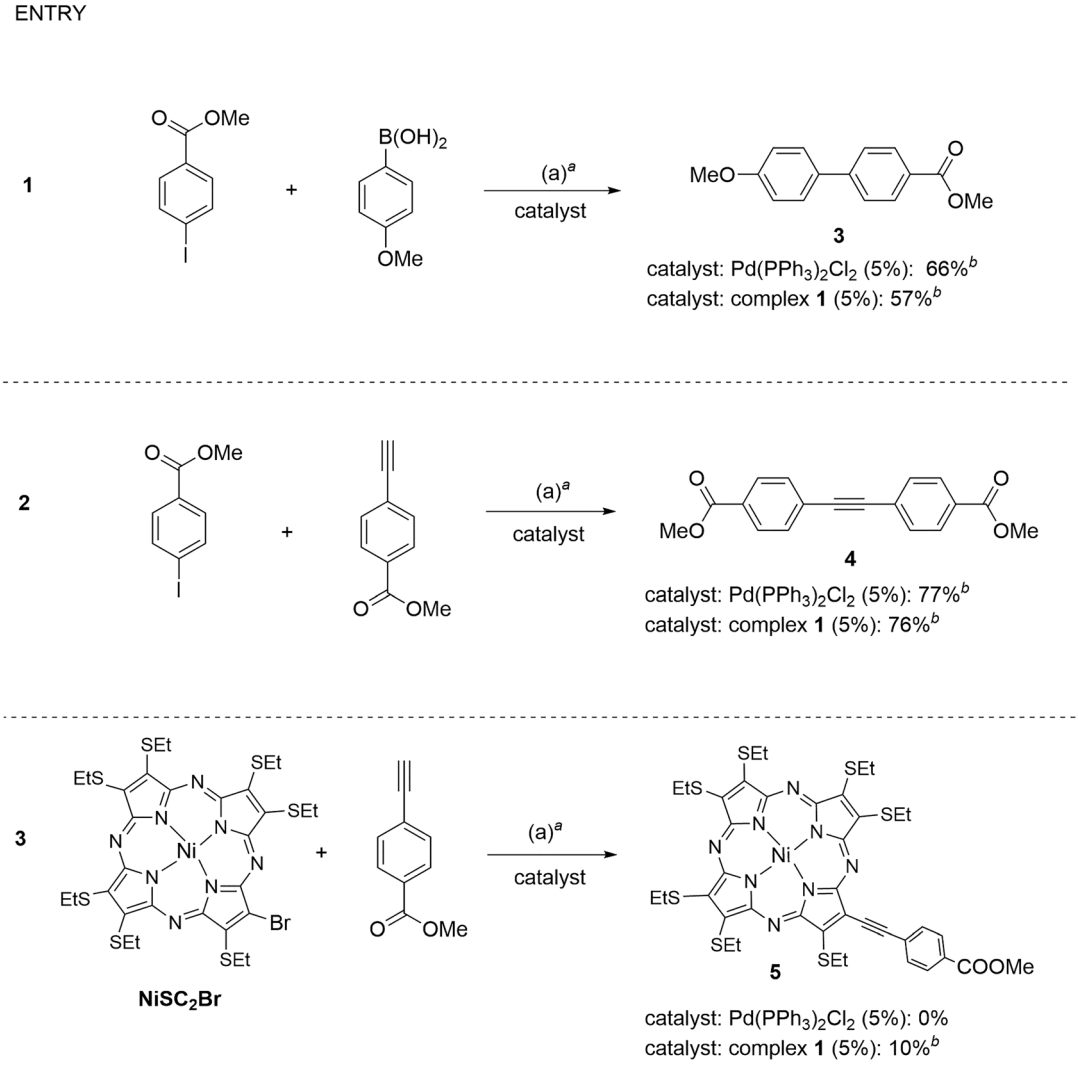

[a]reaction conditions: (a) K_2CO_3 (1.4 equiv.), THF, 60°C, 13h; (b) CuI (0.1 equiv.), Et_3N, 70°C, 14h; (c) CuI (0.1 equiv.), Et_3N/THF, 100°C, 4h; [b]Isolated yields.

Scheme 3 Catalytic activity of complex **1** in cross-coupling reactions.

agreement with experimental data, confirming the reliability of the computational protocol.

Catalytic activity

To verify that complex **1** is effectively an intermediate in the catalytic cycle of Suzuki–Miyaura cross-coupling between bromo-porphyrazines and boronic acids, a stoichiometric reaction between complex **1** and 1-pyrene boronic acid was performed under previously reported conditions.[9] The coupling product was obtained in a satisfactory 80% yield, confirming the role of complex **1** as an oxidative addition intermediate in the catalytic cycle.

Subsequently, complex **1** was evaluated as a catalytic precursor in other coupling reactions. The catalytic activity of complex **1** in promoting cross-coupling reactions was investigated by testing it in both Suzuki–Miyaura and Sonogashira reactions (Scheme 3).

In the Suzuki–Miyaura coupling of *p*-methoxyphenyl boronic acid with 4-iodomethyl benzoate (entry 1), complex **1** showed comparable activity to the classical $Pd(PPh_3)_2Cl_2$ catalyst, affording product **3** in approximately 60% yield. Similarly, in the Sonogashira coupling of 4-iodomethyl benzoate with 4-ethynylmethyl benzoate, both complex **1** and $Pd(PPh_3)_2Cl_2$ delivered product **4** in 76% and 77% yields, respectively. These results demonstrate comparable catalytic efficiencies of complex **1** and $Pd(PPh_3)_2Cl_2$ in these coupling reactions.

Finally, complex **1** was tested in the Sonogashira coupling between the **NiSC$_2$Br** bromo porphyrazine complex and 4-ethynylmethyl benzoate. Notably, the common $Pd(PPh_3)_2Cl_2$ catalyst was ineffective and failed to produce the desired product **5**. As shown in entry 3, complex **1** instead promoted the coupling reaction, albeit with a modest 10% yield.

Conclusions

Pd-catalyzed cross-coupling reactions represent one of the most versatile tools for the peripheral functionalization of tetrapyrrolic macrocycles with aryl, alkynyl, or vinyl moieties. During the Suzuki–Miyaura reaction of the β-bromo thioethyl porphyrazine derivative, the organometallic complex **1**, originating from the oxidative addition of the bromo-porphyrazine to the palladium (0) complex employed, was unexpectedly isolated. The structure of this η^1 organopalladium complex was elucidated through ^{1}HNMR, ^{13}CNMR and ^{31}PNMR analyses and subsequently confirmed by (SCXRD). Complex **1** thus represents the first η^1 tetrapyrrole organometallic complex in which the metal is coordinated at the β position of the macrocycle rather than at the *meso*-position, as observed in some porphyrin complexes. The spectroscopic and electrochemical properties of this complex were investigated by UV-Vis analysis and cyclic voltammetry and interpreted using TDDFT computations, enabling the assignment of the molecular orbital origin of the main electronic transitions. Notably, whereas in peripherally aryl-substituted thioalkyl porphyrazines a charge transfer HOMO–LUMO electronic transition occurs between the aryl substituent and the macrocycle core, in complex **1** charge transfer transitions localized on the $Pd(PPh_3)_2$ substituent occur at significantly higher energies, in correspondence to the Soret band. Finally, the role of complex **1** in the cross-coupling reaction has been ascertained and its catalytic properties were evaluated in both Suzuki–Miyaura and Sonogashira Pd(II)-catalyzed couplings. In both reactions, complex **1** proved to be an efficient catalyst comparable to the commonly used $Pd(PPh_3)_2Cl_2$ complex.

Experimental section

General

Chemicals and solvents were of reagent grade (Sigma Aldrich). Solvents used in physical measurements were of spectroscopic grade. Column chromatography was performed using silica gel (Merck, Kieselgel 60, 60–230 mesh). Analytical thin layer chromatography (TLC) was performed on silica gel 60 0.5 mm sheets (Macherey–Nagel). ^{1}H (400 MHz) and ^{13}C (100 MHz) spectra were recorded in $CDCl_3$ using a Varian INOVA 400 spectrometer, with $SiMe_4$ as an internal standard. UV-vis spectra were recorded in the 250–800 nm range using a UV-vis/NIR Jasco V-770 spectrophotometer in quartz cells with a path length of 1 cm and a solution of *ca.* 10^{-6} M, at a scan rate of 600 nm min^{-1}. The cyclic voltammetry (CV) and differential pulse voltammetry (DPV) experiments were performed with an EG & G Princeton Applied Research Model 263A potentiostat/galvanostat. Data were collected and analyzed using the Model 270 electrochemical analysis system software.[31] A standard three-electrode arrangement was employed. The working electrode was a glassy carbon button (∅ = 3 mm). A platinum wire served as the counter electrode and a home-made AgCl/Ag electrode containing saturated KCl was used as the reference electrode. All the oxidation and reduction potentials are reported relative to the ferrocene/ferrocenium (Fc/Fc^+) potential scale, using the voltammetric oxidation of ferrocene as an internal reference. The reproducibility of individual potential values was within ±5 mV. All the electrochemical measurements were carried out using the Schlenk technique (N_2) at room temperature. The concentration of the supporting electrolyte $[N(C_4H_9\text{-}n)_4BF_4]$ was typically 0.15 M. Cyclic voltammograms were recorded by scanning the potential at 200 mV s^{-1}. DPV measurements were performed at 5 mV s^{-1} with a pulse height of 50 mV and a pulse width of 50 ms. SCXRD data were measured in flowing N_2 at 173 K using a Bruker-Nonius Kappa CCD four-circle diffractometer equipped with an Oxford Cryostream-700 apparatus (graphite monochromated MoKα radiation, λ = 0.71073 Å, CCD rotation images, thick slices, ϕ and ω scans to fill the asymmetric unit). Further details are reported in the ESI.†

Syntheses

[2-(Bromo)-3,7,8,12,13,17,18-heptakis(ethylthio)-5,10,15,20-porphyrazine] (**H$_2$SC$_2$Br**) was prepared as previously described.[18]

2-[Bromo-*trans*-bis(triphenylphosphino)-palladium(II)]3,7,8,12,13,17,18-heptakis (ethylthio)-5,10,15,20–21*H*,23*H* porphyr-

azine (1). Compound H_2SC_2Br (70 mg; 0.086 mmol) was dissolved in 35 mL of anhydrous toluene. Then $Pd(PPh_3)_4$ (95 mg; 0.082 mmol) was added to the solution. The mixture was heated at reflux, checked by TLC and stopped after approximately 40 minutes. Excess solvent was removed under reduced pressure and the crude product was purified on a silica gel column using CH_2Cl_2 : *n*-hexane 7 : 3, v : v mixture and then by preparative TLC with the same eluent mixture. Complex **1** was isolated by collecting the second eluted band (R_f = 0.17). Exchange of the Br atom with Cl took place during the chromatographic purification with CH_2Cl_2 solvent. The first band (R_f = 0.37) was then collected corresponding to the analogous complex **1** containing the Cl atom instead of Br. The collected first and second bands provided **1** in 80% overall yield. ^{1}H NMR (400 MHz, $CDCl_3$), δ/ppm: −1.85 (s, 2H, Np*H*), 1.10 (t, J = 7.6 Hz, 3H, CH_3), 1.41 (t, J = 7.6 Hz, 3H, CH_3), 1.43 (t, J = 7.6 Hz, 3H, CH_3), 1.5–1.7 (m, 12 H, CH_3), 3.75 (q, J = 7.6 Hz, 2H, SCH_2), 3.89 (q, J = 7.6 Hz, 2H, SCH_2), 3.95 (q, J = 7.6 Hz, 2H, SCH_2), 4.0–4.2 (m, 8H, SCH_2), 6.6–6.7 (m, 6H, Ph *p*-H), 6.7–6.8 (m, 12H, Ph *m*-H), 7.6–7.8 (m, 12H, Ph *o*-H). ^{13}CNMR (100 MHz, $CDCl_3$), δ/ppm: 14.98(*C*H_3), 15.49(*C*H_3), 15.57(*C*H_3), 15.65(*C*H_3), 15.73(*C*H_3), 29.32 (*C*H_2), 29.49 (*C*H_2), 29.69 (*C*H_2), 29.84 (*C*H_2), 127.31 (s, Ph *m*-*C*), 129.63 (s, Ph *p*-*C*), 130.40 (t, Ph *ipso*-*C*), 134.48 (t, Ph *o*-*C*), 137.00, 137.17, 139.50, 140.83, 141.93, 142.92, 143.42, 144.81, 147.37, 152.08, 159.67, 159.88, 161.20, 162.25, 165.91, 169.28. ^{31}PNMR (162 MHz, $CDCl_3$), δ/ppm: 24 (s). UV-Vis (CH_2Cl_2), $\lambda_{max.}$ nm^{-1} 307, 363 (Soret), 515 (extra band), 650 and 693 (Q bands).

Computational details

H_2SC_2 geometry has been taken from our previous work[24] while the geometry of complex **1** has been taken from the SCXRD coordinates and further optimized at DFT/B3LYP/def2-svp/gas phase by substituting, for simplicity, the pendant ethyl groups with methyl moieties. No negative frequencies were found suggesting that a real minimum is obtained. Both structures were subjected to TDDFT calculations at the ωB97X-D3/def2-TZVP/CPCM(DCM) level of theory, taking into account the first 100 states using ORCA 6 software.[32] The molecular orbitals have been generated with the use of Avogadro 2 software.[33] The ωB97X-D3 functional[34] is a modern long-range corrected hybrid density functional with improved dispersion corrections. TDDFT/M06/def2-TZVP/CPCM(CH_2Cl_2) and (DMF) levels of theories have been used for HOMO and LUMO energy calculations for comparing with experimental electrochemical data.

Author contributions

Project conceptualization and management were performed by S. B. Investigation and data collection were carried out by S. B., G. L., E. S., A. S. and A. T. Formal analysis was performed by E. S. and A. T. Project supervision and funding acquisition were provided by S. B. The article was written by S. B., E. S. and A. T.

Conflicts of interest

There are no conflicts to declare.

Data availability

The data supporting this article have been included as part of the ESI.†

Crystallographic data for **1** have been deposited at the Cambridge Crystallographic Data Centre under accession number CCDC 2455381† and can be obtained from **https://www.ccdc.cam.ac.uk/data_request/cif**.

Acknowledgements

S. B. and G. L. gratefully acknowledge the financial support from the European Union NextGenerationEU and the Italian Ministry of University (MUR) National Recovery and Resilience Plan (NRRP) Program "Strengthening of research structures and creation of R&D *innovation ecosystems*" (Tech4You – Technologies for climate change adaptation and quality of life improvement Project grant n. ECS_0000009).

References

1 G. de la Torre, P. Vazquez, F. Agullo-Lopez and T. Torres, *Chem. Rev.*, 2004, **104**, 3723–3750.
2 (*a*) M. G. Walter, A. B. Rudine and C. C. Wamser, *J. Porphyrins Phthalocyanines*, 2010, **14**, 759–792; (*b*) B. Sekaran and R. Misra, *Coord. Chem. Rev.*, 2022, **453**, 214312; (*c*) S. Wu and J. Cao, *J. Coord. Chem.*, 2022, 1–26; (*d*) J. M. Park, J. H. Lee and W.-D. Jang, *Coord. Chem. Rev.*, 2020, **407**, 213157; (*e*) G. Di Carlo, A. Orbelli Biroli, M. Pizzotti and F. Tessore, *Front. Chem.*, 2019, **7**, 177; (*f*) A. Mahmood, J.-Y. Hu, B. Xiao, A. Tang, X. Wang and E. Zhou, *J. Mater. Chem. A*, 2018, **6**, 16769–16797.
3 (*a*) G. Bottari, G. de la Torre, D. M. Guldi and T. Torres, *Chem. Rev.*, 2010, **110**, 6768–6816; (*b*) B. H. Lessard, *ACS Appl. Mater. Interfaces*, 2021, **13**, 31321–31330; (*c*) A. M. Schmidt and M. J. F. Calvete, *Molecules*, 2021, **26**, 2823; (*d*) M. Urbani, M.-E. Ragoussi, M. K. Nazeeruddin and T. Torres, *Coord. Chem. Rev.*, 2019, **381**, 1–64; (*e*) G. de la Torre, G. Bottari and T. Torres, *Adv. Energy Mater.*, 2017, **7**, 1601700.
4 E. Annoni, M. Pizzotti, R. Ugo, S. Quici, T. Morotti, M. Bruschi and P. Mussini, *Eur. J. Inorg. Chem.*, 2005, **2005**, 3857–3874.
5 For NLO studies of non-symmetric porphyrazines see: (*a*) S. Vagin, G. Y. Yang, M. K. Y. Lee and M. Hanack, *Opt. Commun.*, 2003, **228**, 119–125; (*b*) S. Vagin and M. Hanack, *Eur. J. Org. Chem.*, 2002, 2859–2865.
6 (*a*) J. Fernández-Ariza, M. Urbani, M. S. Rodríguez-Morgade and T. Torres, *Chem. – Eur. J.*, 2018, **24**, 2618–2625; (*b*) Y. Miyoshi, T. Fujimoto, H. Yoshikawa, M. M. Matsushita,

K. Awaga, T. Yamada and H. Ito, *Org. Electron.*, 2011, **12**, 239–243; (*c*) H. Mori, E. Miyazaki, I. Osaka and K. Takimiya, *Org. Electron.*, 2012, **13**, 1975–1980.

7 (*a*) S. Belviso, M. Amati, R. Rossano, A. Crispini and F. Lelj, *Dalton Trans.*, 2015, **44**, 2191–2207; (*b*) S. Belviso, M. Amati, M. De Bonis and F. Lelj, *Mol. Cryst. Liq. Cryst.*, 2008, **481**, 56–72.

8 S. Belviso, E. Santoro, M. Penconi, S. Righetto and F. Tessore, *J. Phys. Chem. C*, 2019, **123**, 13074–13082.

9 S. Belviso, A. Capasso, E. Santoro, L. Najafi, F. Lelj, S. Superchi, D. Casarini, C. Villani, D. Spirito, S. Bellani, A. E. Del Rio-Castillo and F. Bonaccorso, *Adv. Funct. Mater.*, 2018, **28**, 1705418.

10 S. Belviso, E. Santoro, F. Lelj, D. Casarini, C. Villani, R. Franzini and S. Superchi, *Eur. J. Org. Chem.*, 2018, 4029–4037.

11 S. Belviso, G. Marsico, R. Franzini, C. Villani, S. Abbate and G. Longhi, *Dalton Trans.*, 2022, **51**, 16453–16464.

12 N. Miyaura and A. Suzuki, *Chem. Rev.*, 1995, **95**, 2457–2483.

13 K. Sonogashira, Y. Tohda and N. Hagihara, *Tetrahedron Lett.*, 1975, **16**, 4467–4470.

14 (*a*) D. P. Arnold, Y. Sakata, K.-I. Sugiura and E. I. Worthington, *Chem. Commun.*, 1998, 2331–2332; (*b*) M. J. Hodgson, P. C. Healy, M. L. Williams and D. P. Arnold, *J. Chem. Soc., Dalton Trans.*, 2002, 4497–4504; (*c*) R. D. Hartnell and D. P. Arnold, *Organometallics*, 2004, **23**, 391–399; (*d*) M. J. Hodgson, V. V. Borovkov, Y. Inoue and D. P. Arnold, *J. Organomet. Chem.*, 2006, **691**, 2162–2170; (*e*) M. Y. Jiang, J.-Y. Shin, B. O. Patrick and D. Dolphin, *Dalton Trans.*, 2008, 2598–2602.

15 (*a*) Y. Matano, K. Matsumoto, Y. Nakao, H. Uno, H. Sakaki and H. Imahori, *J. Am. Chem. Soc.*, 2008, **130**, 4588–4589; (*b*) Y. Matano, K. Matsumoto, H. Hayashi, Y. Nakao, T. Kumpulainen, V. Chukharev, N. V. Tkachenko, H. Lemmetyinen, S. Shimizu, N. Kobayashi, D. Sakamaki, A. Ito, K. Tanaka and H. Imahori, *J. Am. Chem. Soc.*, 2012, **134**, 1825–1839.

16 (*a*) S. Belviso, G. Ricciardi and F. Lelj, *J. Mater. Chem.*, 2000, **10**, 297–304; (*b*) G. Ricciardi, S. Belviso, F. Lelj and S. Ristori, *J. Porphyrins Phthalocyanines*, 1998, **2**, 177–188; (*c*) S. Belviso, F. Cammarota, R. Rossano and F. Lelj, *J. Porphyrins Phthalocyanines*, 2016, **20**, 223–233.

17 S. Belviso, G. Ricciardi, F. Lelj, L. Monsù Scolaro, A. Bencini and C. Carbonera, *J. Chem. Soc., Dalton Trans.*, 2001, **29**, 1143–1150.

18 S. Belviso, A. Giugliano, M. Amati, G. Ricciardi, F. Lelj and L. Monsù Scolaro, *Dalton Trans.*, 2004, 305–312.

19 P. S. Pregosin and R. Kunz, *Helv. Chim. Acta*, 1975, **58**, 49–50.

20 (*a*) A. Pidcock, *Chem. Commun.*, 1968, 92–92; (*b*) A. W. Verstuyft, J. H. Nelson and L. W. Cary, *Inorg. Chem.*, 1976, **15**, 732–734.

21 (*a*) G. Ricciardi, A. Bencini, S. Belviso, A. Bavoso and F. Lelj, *J. Chem. Soc., Dalton Trans.*, 1998, 1985–1991; (*b*) G. Ricciardi, A. Bavoso, A. Bencini, A. Rosa, F. Lelj and F. Bonosi, *J. Chem. Soc., Dalton Trans.*, 1996, 2799–2807; (*c*) D. P. Arnold, P. C. Healy, M. J. Hodgson and M. L. Williams, *J. Organomet. Chem.*, 2000, **607**, 41–50.

22 M. Gouterman, *J. Mol. Spectrosc.*, 1961, **6**, 138–163.

23 M. Gouterman, in *The Porphyrins*, ed. D. Dolphin, Academic Press, New York, 1978, vol. 3, 1–165.

24 S. Ghidinelli, S. Abbate, E. Santoro, S. Belviso and G. Longhi, *J. Phys. Chem. B*, 2021, **125**, 264–280.

25 The number of exchanged electrons in each of these redox processes is also confirmed by analyzing the width of the peaks at half height in the corresponding differential small pulse amplitude voltammograms. Considering that in our pulse voltammograms obtained using a pulse amplitude of 50 mV, the measured values of the peak half widths are greater than 90.4 mV, a one-electron reduction process has to be associated with all the studied compounds. See: E. P. Perry and R. A. Osteryoung, *Anal. Chem.*, 1965, **37**, 1634–1637.

26 L. A. Bottomley and W. H. Chiou, *J. Electroanal. Chem.*, 1986, **198**, 331–346.

27 E. A. Ough, K. A. M. Creber and M. Stillman, *Inorg. Chim. Acta*, 1996, **246**, 361–369.

28 Y. Liu, M. S. Liu, X.-C. Li and A. K.-Y. Jen, *Chem. Mater.*, 1998, **10**, 3301–3304.

29 J. Pommerehne, H. Vestweber, W. Guss, R. F. Mahrt, H. Bassler, M. Porch and J. Daub, *Adv. Mater.*, 1995, **7**, 551–554.

30 P. R. Mussini, A. Orbelli Biroli, F. Tessore, M. Pizzotti, C. Biaggi, G. Di Carlo, M. G. Lobello and F. De Angelis, *Electrochim. Acta*, 2012, **85**, 509–523.

31 A. J. Bard and L. R. Faulkner, *Electrochemical Methods, Fundamentals and Applications*, John Wiley & Sons, New York, 1980.

32 F. Neese, *Comput. Mol. Sci.*, 2012, **2**(1), 73–78.

33 (*a*) M. D. Hanwell, D. E. Curtis, D. C. Lonie, T. Vandermeersch, E. Zurek and G. R. Hutchison, *J. Cheminf.*, 2012, **4**, 17; (*b*) Other relevant publications that might be of interest: M. D. Hanwell, W. A. de Jong and C. J. Harris, *J. Cheminf.*, 2017, **9**, 55; (*c*) W. A. de Jong, A. M. Walker and M. D. Hanwell, *J. Cheminf.*, 2013, **5**, 25.

34 Y.-S. Lin, G.-D. Li, S.-P. Mao and J.-D. Chai, *J. Chem. Theory Comput.*, 2013, **9**, 263–272.